buildings

MDPI

Article

Seismic Response of Variable Section Column with a Change in Its Boundary Conditions

Alexandre de Macêdo Wahrhaftig [1,*], Moshe Eisenberger [2,*], Castro Baptista Elias [3] and Luiz Antônio Malheiros Filho [4]

[1] Department of Construction and Structures, Polytechnic School, Federal University of Bahia, 5º Andar, Rua Aristides Novis, 02, Federação, Salvador 40210-910, BA, Brazil
[2] Faculty of Civil and Environmental Engineering, Technion—Israel Institute of Technology, Technion City, Haifa 32000, Israel
[3] Department of Geophysics, Institute of Geosciences, Federal University of Bahia, Rua Barão de Jeremoabo, s/n, Ondina, Salvador 40170-290, BA, Brazil; castroelias@ufba.br
[4] Young Researcher Program, Vice-Rectorate for Research and Graduate Studies, Federal University of Bahia, Rua Basílio da Gama, 6/8, Canela, Salvador 40110-040, BA, Brazil; luiz.malheiros@ufba.br
* Correspondence: alixa@ufba.br (A.d.M.W.); cvrmosh@technion.ac.il (M.E.)

Abstract: The end conditions of columns constitute an important design parameter as they change their stiffness. The degree of restraint of the column modifies its fundamental frequency and mode of vibration. The rotational stiffness at its ends may transform from zero (hinged) to infinite (clamped). For intermediate values, the rotational movement is partially restricted, and it is classified as semi-rigid. In this work, the seismic response for a linearly variable section column and with gradual change in the rotational fixity is studied. A parametric solution is developed using the Rayleigh method, derived for cases of non-prismatic columns, and considering the axially distributed force along the column height. The obtained generalized stiffness and mass are used to perform approximate seismic evaluation at low effort and examine the influence of the changes to the structure. The analysis indicated that with a spring coefficient of 5 EI/l, the displacement drops by 50%, meaning that this range can produce significant influence on the structural response. The relationship between the top load and the column self-weight equal to 0.3 defines the limit for the hinged–hinged boundary condition to exist. As research recommendations, analysis of columns with variable cross-sections and different shapes, different distributed loadings, applying the rotational spring for both ends and over the shape functions, and analysis of buildings by an equivalent system are suggested. Experimental activity is indicated as a possibility for future investigations.

Keywords: variable section columns; support restraints; natural frequency; self-weight; seismic response; Rayleigh's method

check for updates

Academic Editor: Marco Di Ludovico

Received: 17 March 2025
Revised: 15 April 2025
Accepted: 22 April 2025
Published: 25 April 2025

Citation: de Macêdo Wahrhaftig, A.; Eisenberger, M.; Baptista Elias, C.; Malheiros Filho, L.A. Seismic Response of Variable Section Column with a Change in Its Boundary Conditions. *Buildings* **2025**, *15*, 1456. https://doi.org/10.3390/buildings15091456

Copyright: © 2025 by the authors. Licensee MDPI, Basel, Switzerland. This article is an open access article distributed under the terms and conditions of the Creative Commons Attribution (CC BY) license (https://creativecommons.org/licenses/by/4.0/).

1. Introduction

The stiffness of beam-column connections is fundamental in structural analysis, as it affects both the redistribution of forces in frames and the final design of structural elements [1]. These connections are one of the most important components in planning the seismic resistance of frames [2]. Seismic actions are among the deadliest natural disasters and are difficult to predict [3]. Earthquakes originate when the pressure on rocks exceeds their resistance, suddenly releasing the accumulated deformation energy [4]. Due to their unpredictable nature, it becomes challenging to avoid both loss of life and damage to property unless structures are properly designed to withstand the forces resulting from an

earthquake [5]. This can be achieved by finding the adequate level of structural connection stiffness against rotations [6] and by adopting a fixed adequate value [7].

In the context of columns with flexible ends, the conditions of the beam-column and column-foundation connections [8] constitute an important design parameter as they define the way in which these elements connect. A greater or lesser degree of restraint in the ends of the columns modifies their fundamental frequency and the corresponding natural mode of vibration. The foundations connect the superstructure of a building to the ground, transferring the earthquake effect to it primarily through the column joints [9–12].

Experimental tests carried out on reinforced concrete frame joints indicated relative rotations between beams and columns, although they were theoretically classified as rigid. In practice, these rotations lead to reduction of the rigidity of the connections [13,14], including plastic hinge formation [15]. Normally, in monolithic systems, the definition of the level of connection stiffness depends on the inertia of the elements that are connected to each other [16]. This is also the case of structures built with prefabricated components. Although the components are individually built and separate from each other, when they are placed in a structure, they must work together to make the system behave monolithically. This attribute depends entirely on the way connections are confectioned. One way of ensuring monolithic behavior is making the concrete of the joints stronger than that of the precast pier column. In this sense, tests have been performed using ultra-high-performance concrete to seal the joints of a prefabricated structural system. This procedure proved to be extremely favorable when the structure was under seismic excitation [17].

For non-monolithic systems, the restrictions depend on the external fixing mechanisms that provide greater or lesser freedom of rotation in the connection, such as in steel-bolted semi-rigid joints [18], in a beam-column connection with screws and gusset plates [19], in a connection with flush high-strength steel end-plate [20], or in a friction-slip connection of beam-columns, like those used to dissipate the energy of lateral movements caused by earthquakes [21]. In this direction, techniques have been studied to avoid collapse or diminish the effect of mechanisms of failure in structural subsystems. One such technique treats the connection between elements by introducing sliding inner cores, which have been proposed for fully welded joints, achieving improvements up to 70% of resistance [22].

When the rotational stiffening is zero, the support is called hinged, and when the stiffness of the connection is infinite, the connection is clamped. For intermediate values, the connection is classified as semi-rigid, and the rotational movement is partially restricted. Within the scope of the analysis, end constraints are commonly associated with springs, used to simulate the various degrees of stiffness added at the end.

In the field of structural dynamics, the Rayleigh method [23] is an analytical method which uses the principle of conservation of energy to determine the generalized stiffnesses and masses that allow calculation of the natural frequency of vibration of mechanical systems. Wahrhaftig et al. [24] used optimized shape functions by using Rayleigh's method to calculate the fundamental natural frequency of slender steel-reinforced concrete columns. Banerjee and Jackson [25] introduced an innovative dynamic stiffness method to analyze the free vibration of rotating conical Rayleigh beams, focusing on their vibrational characteristics. Ghani et al. [26] investigated the application of Rayleigh's method (classical and modified) for calculating the natural frequency of cantilever beams with inhomogeneous properties.

Peng et al. [27] investigated steel columns made of tube and H-sections, using composite joints of beams of different depths, with the aim of analyzing their shear strength in relation to earthquake damage, concluding that beam height is key factor in joint strength. In their research, Poudel et al. [28] analyzed earthquakes in irregular buildings using linear dynamic analysis and the response spectrum method of time history analysis to obtain

frequencies and structural responses using ETABS software version 16.2.1. Unlike steel joints, the performance of concrete joints is primarily governed by the same principles. Xu et al. [29] used the ABAQUS software version 6.14. to simulate non-linear tests on inclined reinforced concrete and steel beam-column exterior joints, as well as investigating the influence of beam inclination angle, yield stress of the cast steel, volume to stirrup ratio, and steel content on the seismic performance of the joints, which can define the level of rotation of a connection in reinforced concrete structures. That study concluded that the stirrup volume of the beam is not decisive in improving the carrying capacity of the joint, but the reinforcement ratio of the column is. The conclusion emphasizes that for practical engineering, to improve the ultimate bearing capacity and deformation performance of reinforced concrete structural members, it is necessary to increase the internal steel content of the joints.

In this context, the mode of lateral deformation and the distribution characteristics of the drift ratio along the structural height are important for the seismic behavior of the structural system [30]. During an earthquake, seismic forces can produce horizontal movements that lead to lateral deformation. Analyzing the pattern of lateral movement makes it possible to identify the most vulnerable areas of the building, making it possible to implement strengthening measures. Structures that have a balanced distribution of the drift ratio tend to behave better during an earthquake, as the seismic load is dispersed more evenly throughout the structure. This not only improves the safety of the building but also increases occupant comfort by reducing the potential for damage to structures and non-structural elements.

Based on these principles, in this work, results are presented for a linearly variable section column with different base–top ratios, and with gradual change in the restraint levels at one end, from the hinged to clamped. A parametric solution is developed using Rayleigh's method, derived for cases of non-prismatic columns, and considering the axially distributed force coupled to the section variation along the column height. The seismic response is simulated by applying the El Centro earthquake ground accelerations that occurred in 1940 in Southern California.

It is important to highlight that the main novelty of this work concentrates on the evaluation of the response of a column to seismic action with a continuous transition of one of its boundary conditions. The following innovative aspects can also be mentioned: (a) This work makes use of the Rayleigh method, with three innovative approaches being implemented in this respect. The first is the consideration of the self-weight of the column directly within the geometric stiffness parcel of the total generalized stiffness. The second is the gradual adjustment of shape functions of different boundary conditions, which is performed using a regulator associated with the rotational spring coefficient applied to the base connection. Third, analysis of columns with variable cross-sections is performed with low numerical effort; (b) This work also considers the concomitant structural response of a distributed load to a top force. This aspect establishes the maximum ratio between the top concentrated load and the total self-weight of the column for the hinged–hinged boundary condition to exist. The self-weight depends on the density of the material. Therefore, it is possible to define parameters in design and structural analysis based on the parametric results obtained.

2. Essential Parameters of the Analytical Method

The mathematical formulation developed for determining the natural frequency of the columns with gradual transition of support is based on Rayleigh's method [23]. It is important to mention that Rayleigh's method uses the principle of conservation of energy, which states that the total mechanical energy of a vibrating system remains unchanged

and is distributed between kinetic energy and potential energy. These two forms of energy vary over time. When kinetic energy reaches its maximum and minimum values, potential energy, on the other hand, reaches its minimum and maximum values, respectively [31], considering the equilibrium equations and boundary conditions.

For a structural element with variable cross-sections, the original method is used in an innovative way to allow for the solution of non-prismatic columns. Inclusion of the structural element's self-weight is achieved automatically in the geometric stiffness portion. It is worth noting that the inclusion of self-weight in the evaluation of the frequency of vibration is an analytical aspect that deserves to be highlighted given the historical challenges faced in the first studies of the phenomenon [32].

The models in Figure 1 represent non-prismatic columns submitted to concentrated and distributed compressive forces. The parameters of the problem are the concentrated force at the free end, P, the length of the column, l, the modulus of elasticity, E, and the specific weight of the material, γ. The geometric variable proprieties of the columns, such as $I(y)$ and $A(y)$, refer to the moment of inertia related to the direction of the vibratory movement considered and the cross-sectional area, respectively. If a rotational spring with a variable coefficient, k, is inserted to the support at the column base, the column transits gradually from an H–H (hinged–hinged) to a C–H (clamped–hinged) boundary condition, as shown in Figure 2. This operation does not depend on the applied forces, but the structural response does.

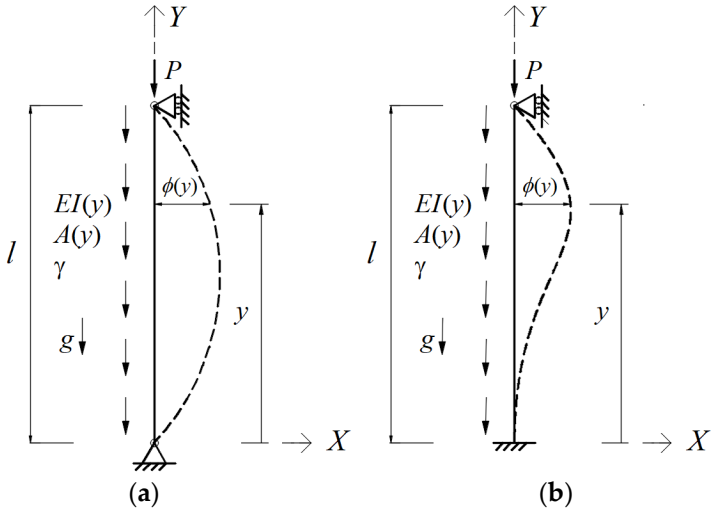


Figure 1. Boundary conditions for the columns models: (**a**) initial, (**b**) final.

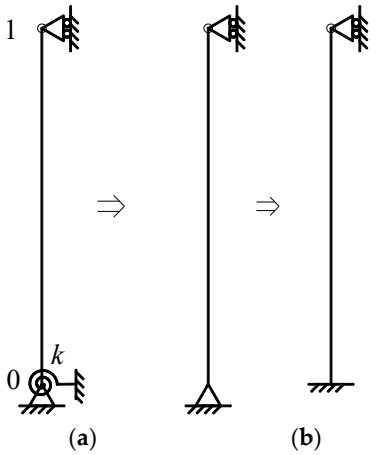


Figure 2. Column with gradual change in its boundary condition from (**a**) initial to (**b**) final.

For the cases shown in Figure 1, the functions assumed for the boundary conditions Figure 1a and Figure 1b, respectively, $\phi_a(y)$ and $\phi_b(y)$, are as follows:

$$\phi_a(y) = \sin\left(\frac{\pi y}{l}\right), \tag{1}$$

and

$$\phi_b(y) = \sin\left(\pi\frac{l-y}{l}\right)\cos\left(\pi\frac{l-y}{l}\right). \tag{2}$$

In order to make a gradual transition from one case of boundary condition to another case, as defined in Figure 2, is necessary to consider that the vibration mode also gradually changes from the initial mode to the final mode, as suggested by Equation (3).

$$\phi(y,k) = \frac{1}{k}\phi_a(y) + \phi_b(y) \tag{3}$$

By applying the principles of virtual work and energy conservation [33], the term of the generalized flexural stiffness is given as follows:

$$K_0(k) = \int_0^l EI(y)\left(\frac{d^2\phi(y,k)}{dy^2}\right)^2 dy, \tag{4}$$

and the generalized geometric stiffness term is given as follows:

$$K_g(k) = \int_0^l N(y)\left(\frac{d\phi(y,k)}{dy}\right)^2 dy, \tag{5}$$

where

$$N(y) = P + \int_y^l A(y)\gamma dy, \tag{6}$$

with $\gamma = \rho$ g, where ρ is the mass density and g is the acceleration of gravity. The column's total self-weight is obtained by solving the integral in Equation (6) in the entire domain of the problem, i.e.,

$$G = \int_0^l A(y)\gamma dy. \tag{7}$$

The generalized stiffness of a rotational spring attached to the columns is given as follows:

$$K_{ri}(k) = k\left(\frac{d\phi(y_i,k)}{dy}\right)^2, \tag{8}$$

where y_i indicates the location of the spring along the column, and k is the rotational stiffness of the spring. In the present case, i can assume only one value, at the base ($y_0 = 0$). The stiffness of the added rotational springs will be taken as:

$$k = \kappa\frac{EI(l)}{l}, \tag{9}$$

where κ is just a number. The function, $\phi(y,k)$, in Equations (4), (5) and (8), is the assumed shape function, and should represent the first vibration mode, obeying the kinematic boundary condition of the problem [34]. The assumption of a shape function transforms the continuous problem into another simplified problem with only one degree of freedom [35],

and the solution is obtained similarly to algebraic eigenvalue problems [36]. Then, the total generalized stiffness of the column is calculated as:

$$K(k) = K_0(k) - K_g(k) + K_{ri}(k) \tag{10}$$

assuming k as an independent variable of the problem. The generalized mass, M, is taken into account by considering the contribution of column self-weight, m^*, and the concentrated mass represented by the force P at position 1, m_P:

$$M(k) = m^*(k) + m_P(\phi(y_P,k))^2, \tag{11}$$

with

$$m^*(k) = \int_0^l \frac{A(y)\gamma}{g}(\phi(y,k))^2 dy, \tag{12}$$

and

$$m_P = \frac{P}{g}. \tag{13}$$

As $y_P = l$ and $\phi(l,k)$ is equal to zero, the effect of the concentrated mass due to the top force on the results vanishes. The natural fundamental frequency of the columns can be calculated assuming the relationship between the total generalized stiffness and mass:

$$\omega(k) = \sqrt{\frac{K(k)}{M(k)}}(\text{in rad}/s) \tag{14}$$

3. Problem Definition

Consider the column with a cross-section varying linearly from the base to the top, as depicted in Figure 3. The variation of the width is given by the ratio $n = b_0/b_1$. The results are given in parametric form as follows.

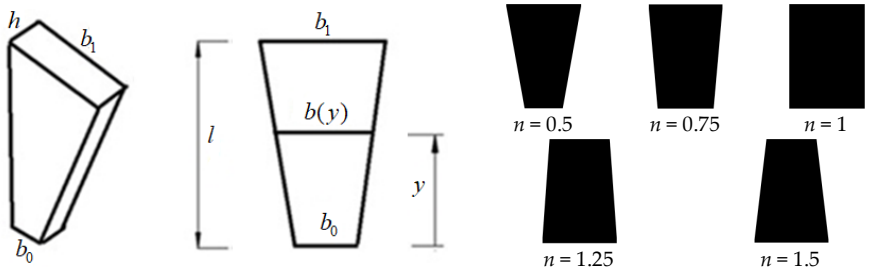


Figure 3. Column with linearly variable cross-section by $n = b_0/b_1$.

The variation of the lateral dimension of the cross-section is given as follows:

$$b(y) = (b_1 - b_0)\frac{y}{l} + b_0 \therefore\ b(y,n) = nb_1 + b_1(1-n)\frac{y}{l} \tag{15}$$

and the cross-sectional area and inertia, respectively, are

$$A(y,n) = b(y,n)h \tag{16}$$

$$I(y,n) = \frac{b(y,n)h^3}{12} \tag{17}$$

where h is the height of the cross-section. When introducing a variable area into the problem, Equations (4)–(7) and (10)–(12) become a function of the relationship between the dimensions of the base and top, n. This way, it can be written that:

$$\omega(k,n) = \sqrt{\frac{K(k,n)}{M(k,n)}} \text{ (in rad/s)} \tag{18}$$

A numerical simulation is conducted to obtain the frequency of five columns, considering that I_1, E, and l are equal to 1 in their correspondent units of the international system of unities (S.I.), and g = 9.80665 m/s^2. All formulations were implemented in Mathcad software version 13.

4. Natural Frequencies of Vibration

The numerical results for the natural frequency of the column, described in Equation (18), consider that the concentrated force at the free end, P, assumes values equal to 0, 1.32, and 2.64, and that the parameter, n, which governs the variation in the width along the column, assumes values within the range of 0.5 to 1.5. The column's self-weight, G, is presented in Table 1. The buckling critical load for P and G that take to the nullity of Equation (10) can be seem in Table 2, where P_{cr} was obtained for G equal to zero and q_{cr} for when P is absent. The results are compared to the values from an analytical procedure based on expansion in series as given in ref. [37], where P_{cr} as q_{cr} are given in a normalized form. Therefore, it is possible to see that all the values of P are far from the force that leads the column to buckle. The relationship between the highest P (=2.64) by the first buckling load P_{cr} (=7.26, exact), represents a ratio P/P_{cr} equal to 0.36. The highest ratio G/q_{cr} is 0.633 (G = 11.768; q_{cr} = 18.569, exact).

Table 1. Column's self-weight (G). Values in "N".

n	ρ		
	0.001	**0.01**	**0.1**
0.50	0.074	0.735	7.355
0.75	0.103	0.883	8.826
1.00	0.118	1.177	11.768
1.25	0.132	1.324	13.239
1.50	0.147	1.471	14.710

Table 2. Critical buckling load [37]. Values in "N".

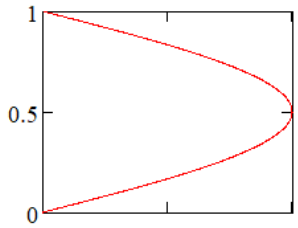
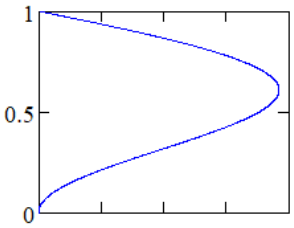
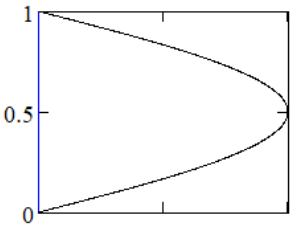
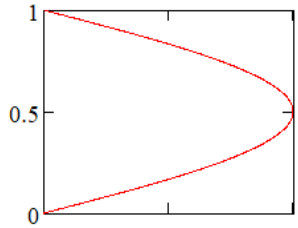
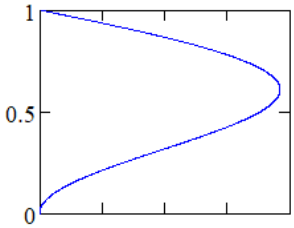
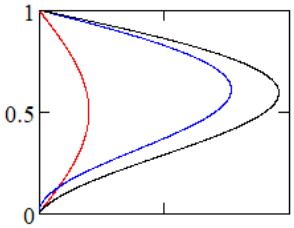
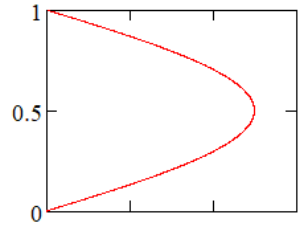
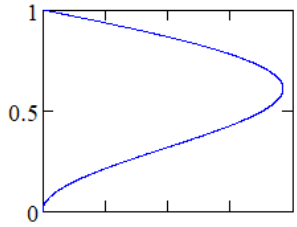
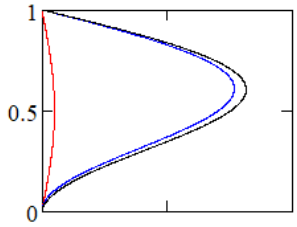
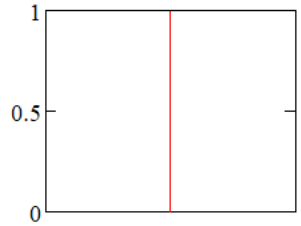
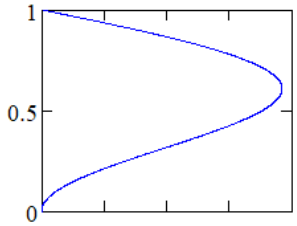
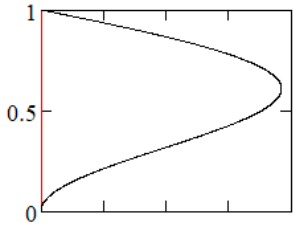
n	Method	k = 0		k = 1		k = 5		k = 20		k = ∞	
		P_{cr}	q_{cr}	P_{cr}	q_{cr}	P_{cr}	q_{cr}	P_{cr}	q_{cr}	P_{cr}	q_{cr}
0.50	Rayleigh	7.40	13.74	10.22	22.81	13.45	33.81	14.81	38.32	15.37	40.11
	Exact	7.26	12.80	9.14	17.18	12.13	25.82	17.07	47.31	14.72	34.88
0.75	Rayleigh	8.64	16.72	11.46	27.03	15.33	41.14	19.33	56.60	17.80	49.82
	Exact	8.61	15.75	10.40	20.04	13.81	30.03	21.58	66.12	17.58	43.93
1.00	Rayleigh	9.87	19.74	12.71	31.29	17.21	48.66	23.84	75.82	20.23	59.88
	Exact	9.87	18.57	11.60	22.79	15.28	33.64	14.81	38.32	20.19	52.50
1.25	Rayleigh	11.10	22.79	13.96	35.57	19.09	56.32	17.07	47.31	22.66	70.22
	Exact	11.08	21.30	12.75	25.46	16.62	36.93	19.33	56.60	22.65	60.75
1.50	Rayleigh	12.34	25.87	15.21	39.88	20.97	64.09	21.58	66.12	25.09	80.77
	Exact	12.25	23.97	13.88	28.09	17.87	40.01	23.84	75.82	25.00	68.80

$P_{cr} = \hat{P}(EI(l)\backslash l), q_{cr} = \hat{q}(EI(l)\backslash l^3)$.

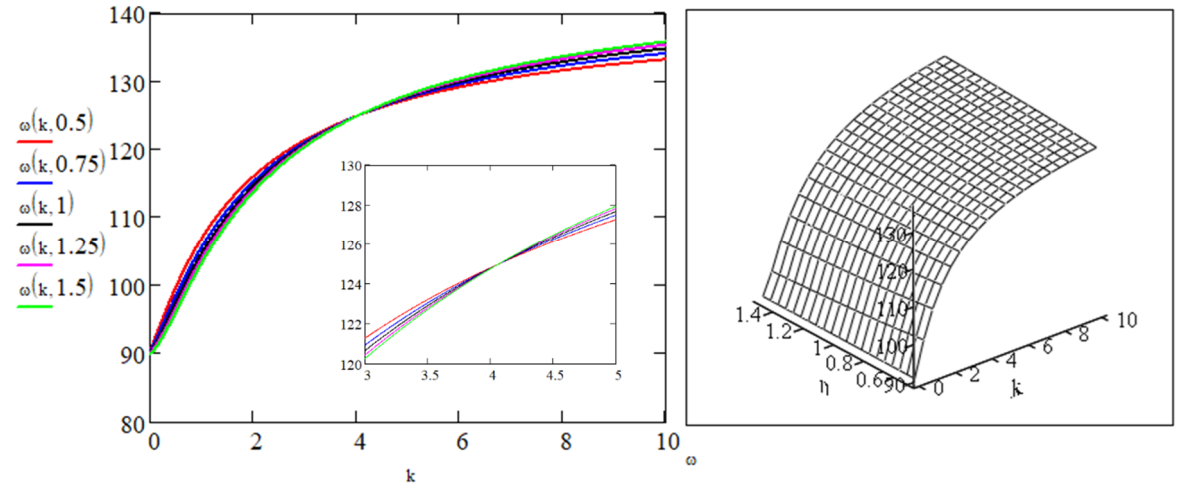
Next, we show the employment of Equation (18) with different values of the concentrated load at the top, P, and the density of the material, ρ, when they act simultaneously. In this case, α, represents the ratio of the top load to the total self-weight, P/G, for a given value of n. The following parameters are considered: (a) the density of the material is equal to 0.001, 0.01, and 0.1; (b) the rotational spring coefficient, k, varies independently; (c) the relationship between the dimension of the base and the top, n, assumes the values indicated previously.

The evolution of the shape function according to Equation (3) is presented below for some specific representative values of k in Table 3. The results for the frequency are shown in Figures 4–6, considering the variation in the rotational stiffness coefficient from zero up to 10 (left side). Also, on the right, the frequency variations as n and k are taken in the range of 0.5 to 1.5 and 0 to 10, respectively, are presented. The results are given for three levels of top loading (0, 1.32, and 2.64) and for three levels of self-weight (0.001, 0.01, and 0.1).

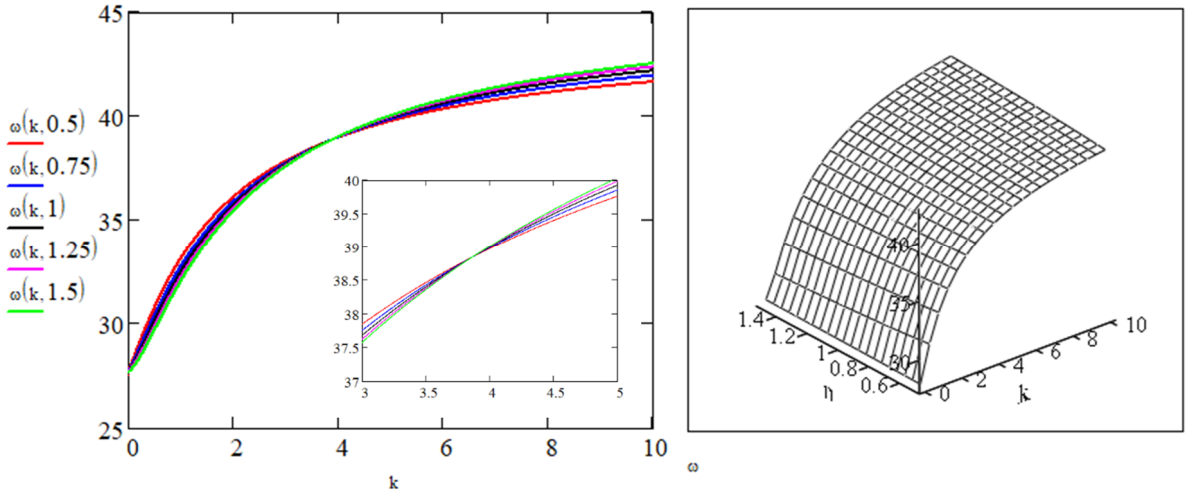
Table 3. Evolution of shape functions.

k	(a) $\frac{1}{k}\phi_a(y)$	(b) $\phi_b(y)$	(c) $\phi(y,k)$
0			
5			
20			
∞			

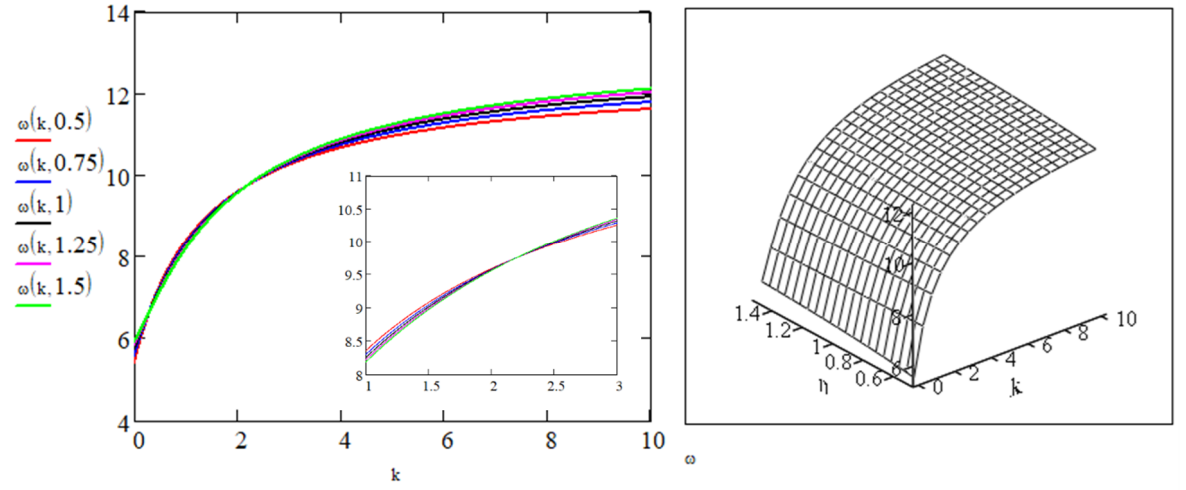
- $P = 0$



(**a**)



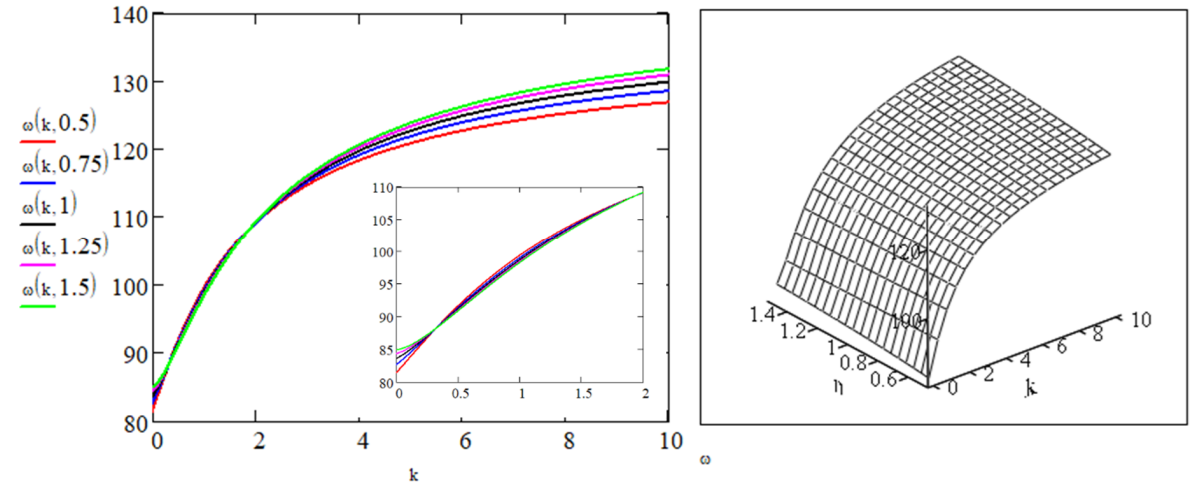
(**b**)



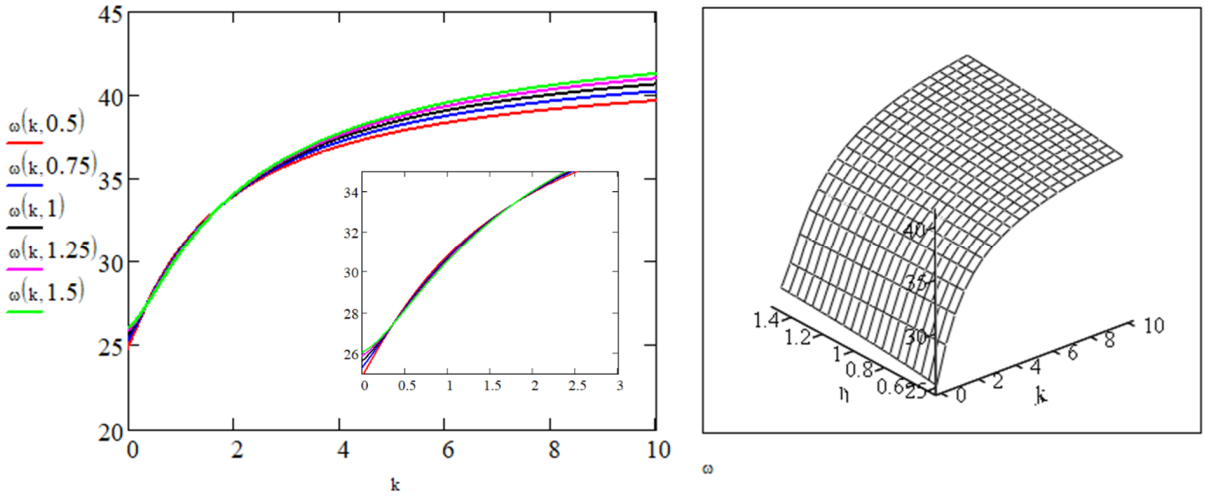
(**c**)

Figure 4. Results for the first natural frequency of the columns for $P = 0$. (**a**) $\rho = 0.001$: $\alpha = 0$ for all n. (**b**) $\rho = 0.01$: $\alpha = 0$ for all n. (**c**) $\rho = 0.1$: $\alpha = 0$ for all n.

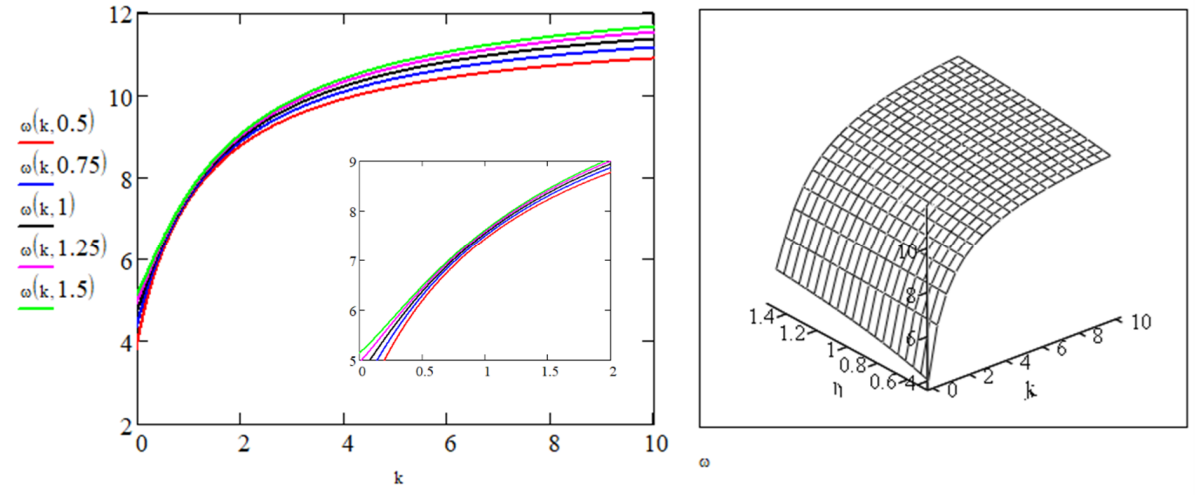
- $P = 1.32$



(**a**)



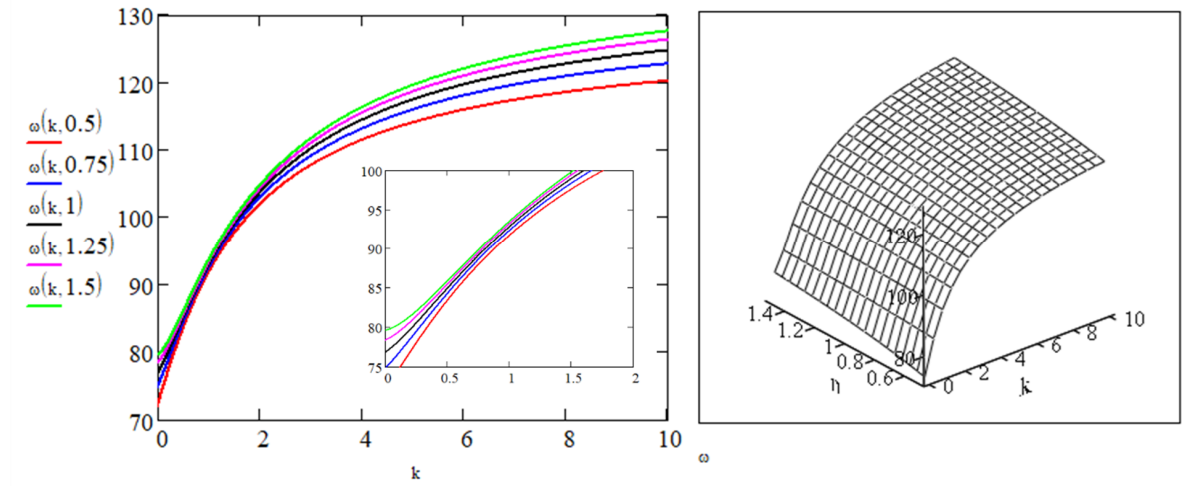
(**b**)



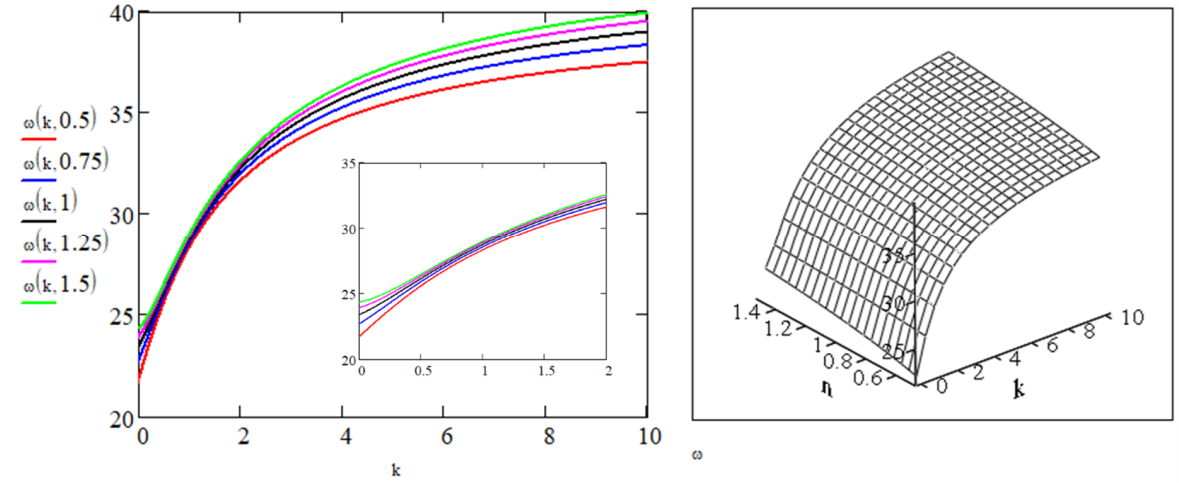
(**c**)

Figure 5. Results for the first natural frequency of the columns for $P = 1.32$. (**a**) $\rho = 0.001$: α (0.5) = 14.96, α (0.75) = 12.82, α (1.0) = 11.22, α (1.25) = 9.97, α (1.5) = 8.97. (**b**) $\rho = 0.01$: α (0.5) = 1.50, α (0.75) = 1.28, α (1.0) = 1.12, α (1.25) = 1.00, α (1.5) = 0.90. (**c**) $\rho = 0.1$: α (0.5) = 0.15, α (0.75) = 0.13, α (1.0) = 0.11, α (1.25) = 0.10, α (1.5) = 0.09.

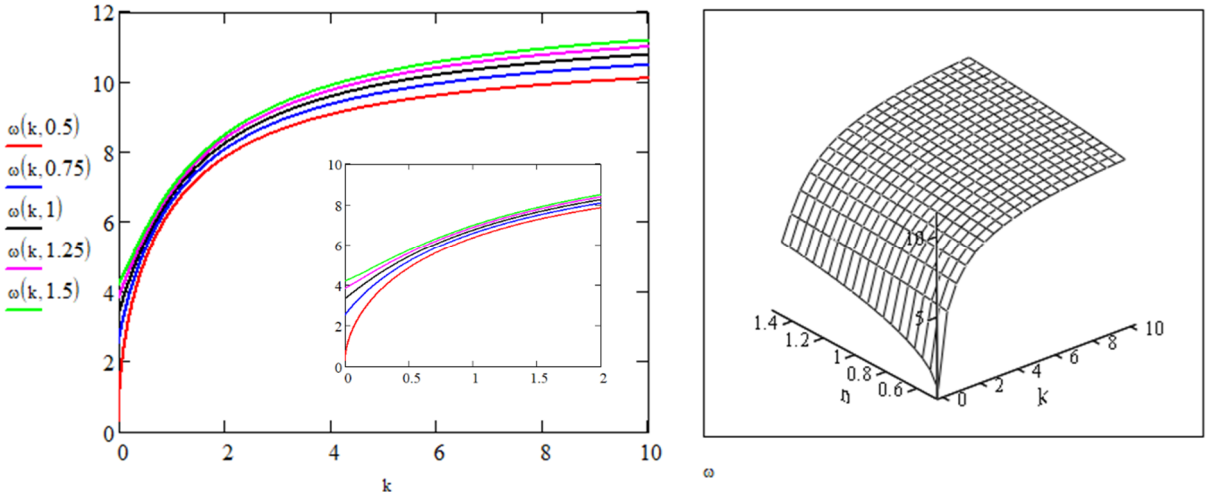
- $P = 2.64$



(**a**)



(**b**)



(**c**)

Figure 6. Results for the first natural frequency of the columns for $P = 2.64$. (**a**) $\rho = 0.001$: α (0.5) = 29.91, α (0.75) = 25.64, α (1.0) = 22.43, α (1.25) = 19.94, α (1.5) = 17.95. (**b**) $\rho = 0.01$: α (0.5) = 2.99, α (0.75) = 2.56, α (1.0) = 2.24, α (1.25) = 1.99, α (1.5) = 1.79. (**c**) $\rho = 0.1$: α (0.5) = 0.30, α (0.75) = 0.26, α (1.0) = 0.22, α (1.25) = 0.20, α (1.5) = 0.18.

The numerical results obtained for the natural frequency of columns with variable cross-sections, as described by Equation (18), reveal a strong dependence on geometric properties, boundary conditions, and the magnitude of the axial loads. The increase in the spring coefficient, k, from zero to infinity does not represent greater natural frequencies because it depends on the association of P, ρ, and n. Particular situations are described below.

For $P = 0$, the frequency for $n = 1.5$ is smaller than that for the other n, reversing when k increases. This is a characteristic behavior independent of the density adopted. However, for ρ equal to 0.001 and 0.01, this reversion occurs for k around 4, and at 3 for ρ equal to 0.1.

For $P = 1.32$, the frequency for $n = 1.5$ starts higher than for the other n values. When k is equal to about 0.3, this situation inverts, with the frequency for the higher-value n becoming the lowest. For k equal to around 2, another switch occurs, and the frequency for the larger n becomes the highest. This last behavior remains unchanged for the whole range of k. This is a pattern which characterizes the density of 0.001 and 0.01. For the density of 0.1 (heavy column), the frequency for the large n always increases with k.

For $P = 2.64$, the frequency always grows with k, independently of ρ and n. For this value of P, the top force reaches a maximum because the self-weight causes the column with $k = 0$ (hinged–hinged) to buckle. This value corresponds to 36% of the lowest critical buckling load. In the condition near the buckling, the ration between P and G is 0.3.

Table 4 summarizes the results obtained for frequency according to the normal force acting on the system. In Table 4, it is possible to see that the frequency decreases in a non-linear way according to the density of the material for the same top force applied. When the density of the material increases by ten times, the frequency of the column decreases by around three times in relation to the previous value. For the same density, when the column changes shape, the frequency grows by different percentages. For $P = 0$, they are 1.91, 2.07, and 4.05. For $P = 1.32$, these values are 3.71, 3.93, and 6.60. For $P = 2.64$, they are 5.79, 6.06, and 9.65.

Table 4. Frequency variation according to the normal force ($k = 10$).

P (N)	ρ (kg/m^3)	G (N)		α		w (rad/s)		w Variation (%)		
		n		n		n		n		
		0.5	**1.5**	**0.5**	**1.5**	**0.5**	**1.5**	**0.5**	**1.5**	**0.5/0.75**
0	0.001	0.09	0.15	0	0	133.16	135.75	-	-	1.91
	0.01	0.88	1.47	0	0	41.65	42.53	68.72	68.67	2.07
	0.1	8.83	14.71	0	0	11.62	12.11	72.10	71.53	4.05
1.32	0.001	0.09	0.15	14.67	0.07	126.85	131.74	-	-	3.71
	0.01	0.88	1.47	1.50	0.01	39.63	41.25	68.76	68.69	3.93
	0.1	8.83	14.71	0.15	0.00	10.89	11.66	72.52	71.73	6.60
2.64	0.001	0.09	0.15	29.33	0.07	120.22	127.61	-	-	5.79
	0.01	0.88	1.47	3.00	0.01	37.51	39.93	68.80	68.71	6.06
	0.1	8.83	14.71	0.30	0.00	10.11	11.19	73.05	71.98	9.65

5. Response to Seismic Action

The seismic response used in this work is the North-South component of the El Centro earthquake of 18 May 1940. The accelerations and the spectrum of frequencies are shown in Figure 7a,b.

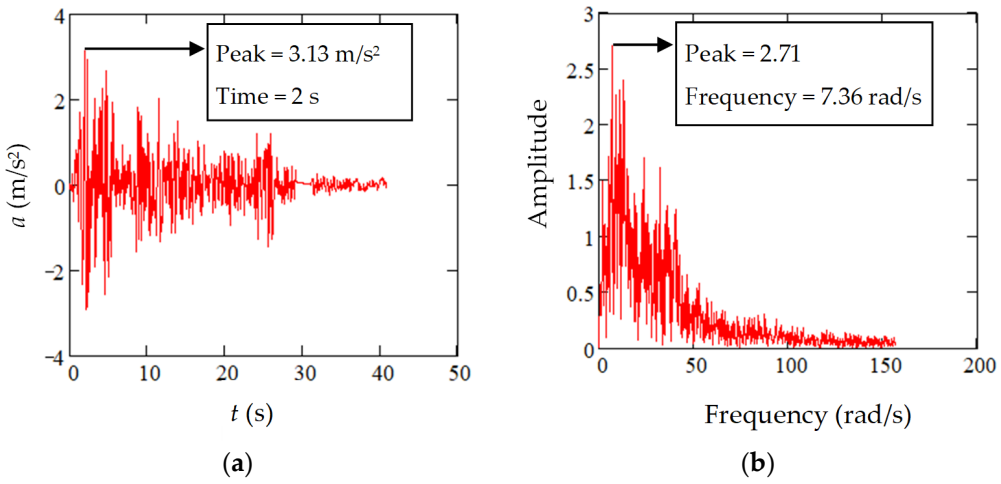


Figure 7. Seismic action: (**a**) time series acceleration, (**b**) spectrum of frequencies (FFT).

5.1. Generalized Structural Displacement

It is important to note that by using the analytical method previously presented, the stiffness and mass of the structure are obtained in terms of the generalized coordinate, which depends on the shape function defined to represent the vibration mode considered. Therefore, when the column transits from the first boundary condition to the second one, the shape function continually transits from one to the other, altering the structural response for both endpoint values and between these.

Using this mathematical approach, both stiffness and the structural mass are obtained directly from the continuum, making it possible to represent a system with an infinite number of degrees of freedom (MDOF) by another equivalent containing only a single one (SDOF). Thus, with the generalized mass, the inertial forces can be obtained by considering that $F = Ma$. Based on these forces, the generalized structural displacements are found in sequence by $u = F/K$. With this in mind, we can see that the generalized structural deflection, u, by the generalized coordinate as a function of time is shown in Figures 8–10 according to the shape of the column and assumed rotational stiffness, k. The results are shown for the critical top load, and the mass density as in the previous analysis.

- $P = 2.64$
  - $\rho = 0.001$

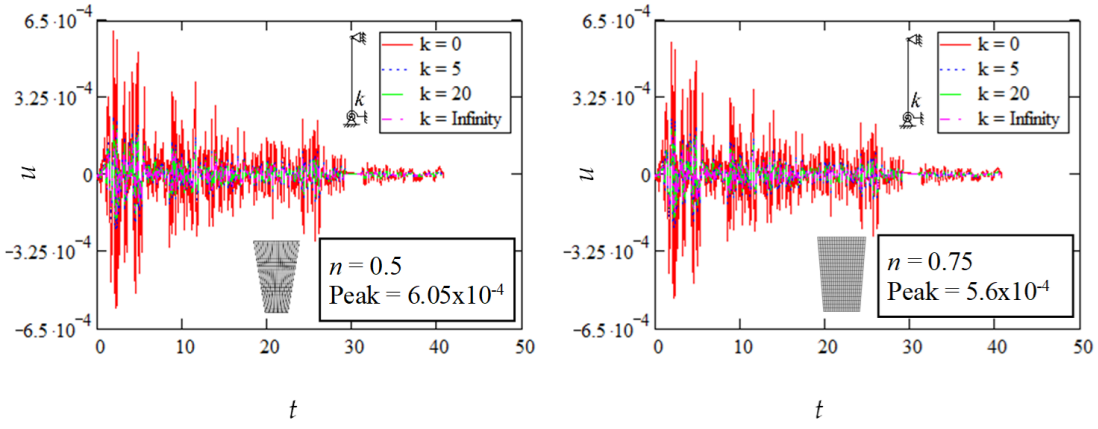


Figure 8. *Cont.*

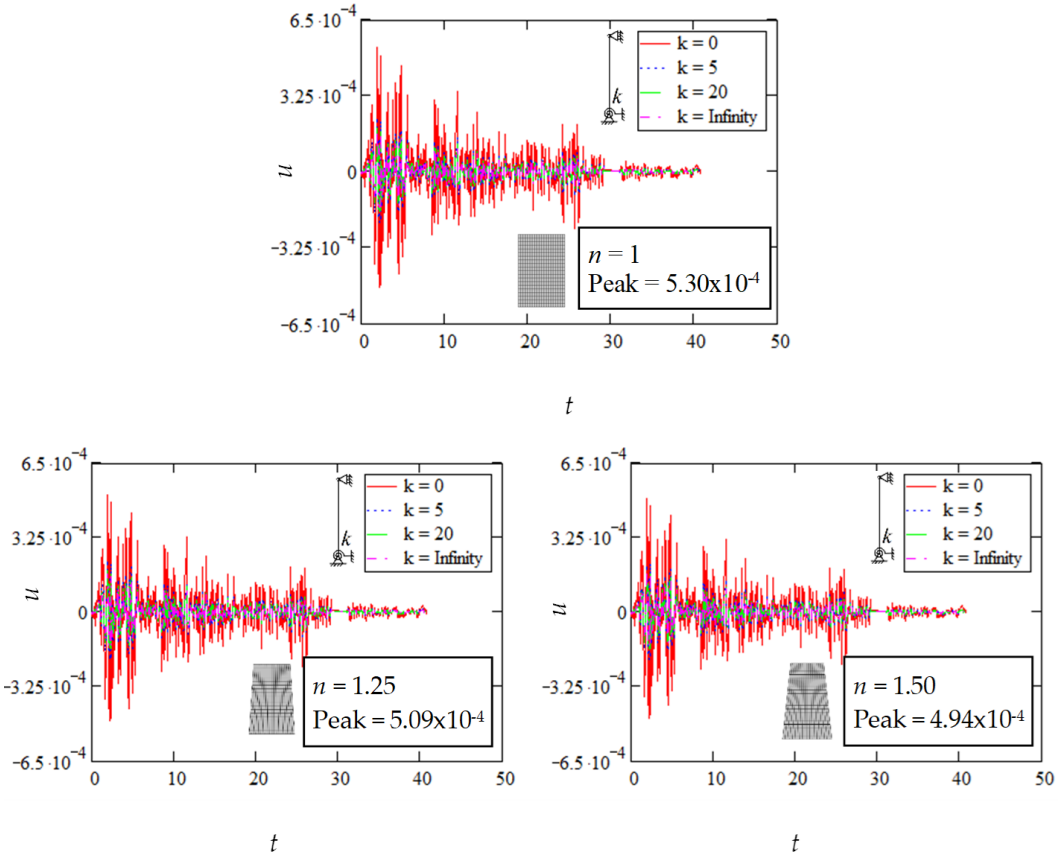


Figure 8. Structural response in terms of the generalized displacement in time: $P = 2.64$, $\rho = 0.001$. k is the rotational spring coefficient.

- $\rho = 0.01$

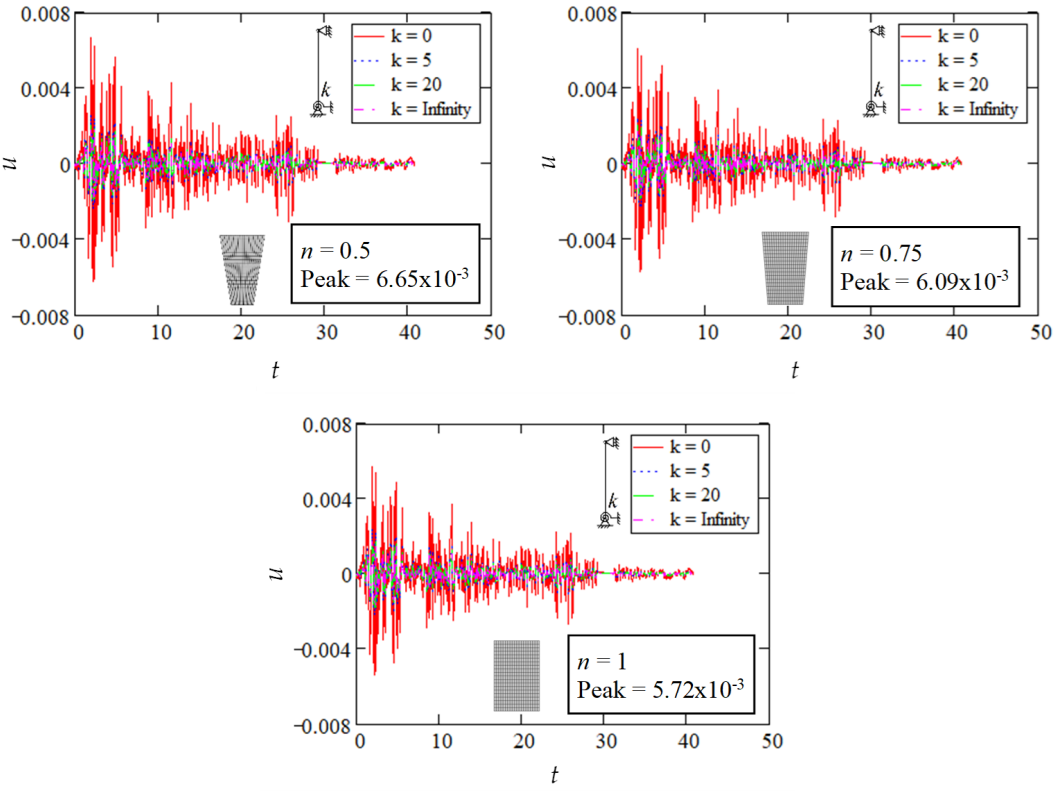


Figure 9. *Cont.*

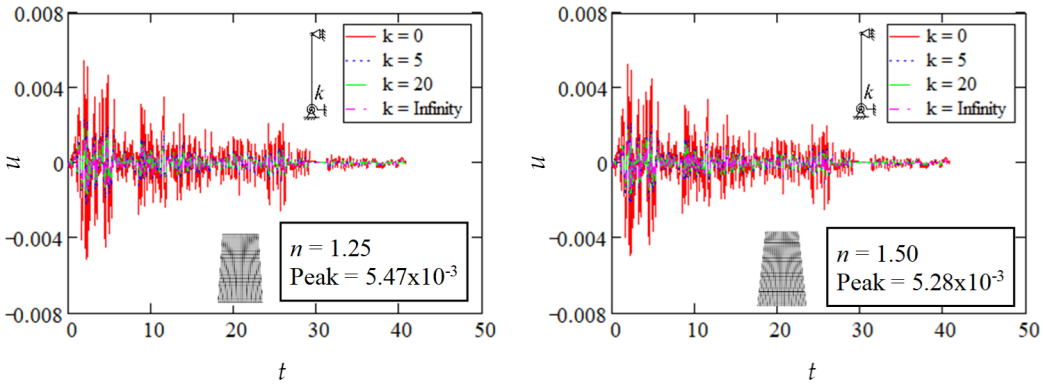


Figure 9. Structural response in terms of the generalized displacement in time: $P = 2.64$, $\rho = 0.01$. k is the rotational spring coefficient.

- $\rho = 0.1$

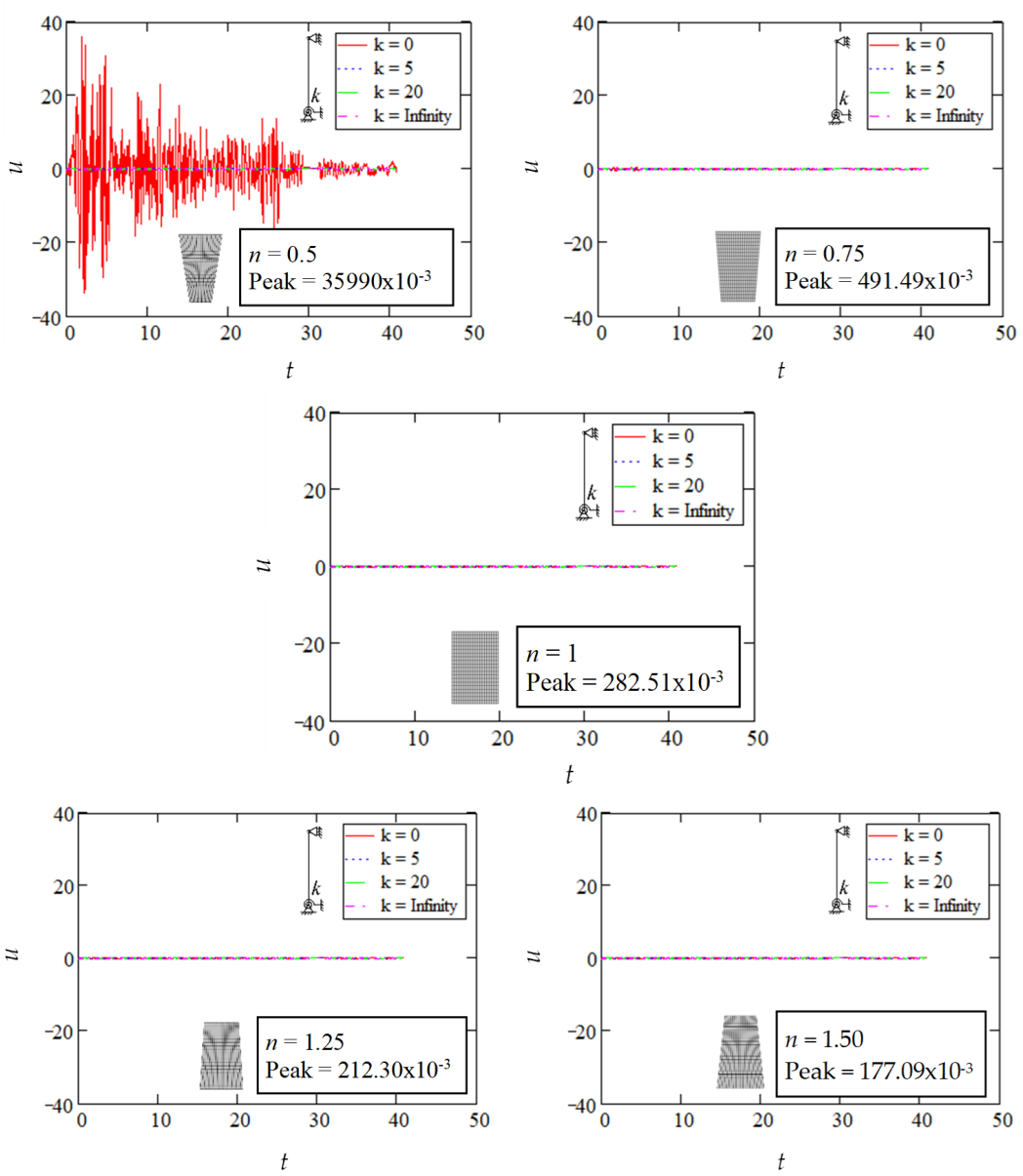


Figure 10. Structural response in terms of the generalized displacement in time: $P = 2.64$, $\rho = 0.1$. k is the rotational spring coefficient.

5.2. Peak Structural Movement

Based on the earthquake peak acceleration, the structural response can be obtained. In this context, the structural motion is described by means of its peak displacement, peak velocity, and peak acceleration, considering both the rotational spring coefficient, k, and the ratio between base and top dimensions, n. Velocity and acceleration are obtained by taking the first and second derivatives of the displacement, u.

Tables 5–7 summarize the peak structural response of displacement, velocity, and acceleration, respectively, for three levels of top loading and three material densities, ρ. It is possible to see that for each ratio n (base and top dimensions), the small added rotational stiffness coefficient results in higher displacements, and that the top load also has a major effect. Therefore, for the same P, increasing k, the displacements diminish. Increasing ρ, the displacements increase. Increasing P, the displacements always increase for the same condition of k and ρ. The peak velocity follows the same pattern as before and acceleration peak follows the inverse behavior except when near the buckling.

Table 5. Displacement response.

n	k	**Peak Displacement**								
		$P = 0$			$P = 1.32$			$P = 2.64$		
		$\rho = 0.001$ ($\times 10^{-4}$)	$\rho = 0.01$ ($\times 10^{-3}$)	$\rho = 0.1$ ($\times 10^{-3}$)	$\rho = 0.001$ ($\times 10^{-4}$)	$\rho = 0.01$ ($\times 10^{-3}$)	$\rho = 0.1$ ($\times 10^{-3}$)	$\rho = 0.001$ ($\times 10^{-4}$)	$\rho = 0.01$ ($\times 10^{-3}$)	$\rho = 0.1$ ($\times 10^{-3}$)
0.5	0	3.88	4.12	107.67	4.72	5.09	214.70	6.05	6.65	35,990.00
	5	1.99	2.04	27.23	2.22	2.28	31.62	2.50	2.58	37.70
	20	1.69	1.72	21.95	1.86	1.90	24.87	2.06	2.11	28.68
	∞	1.58	1.61	20.16	1.72	1.76	22.66	1.90	1.95	25.85
0.75	0	3.88	4.10	100.29	4.58	4.90	166.58	5.60	6.09	491.49
	5	1.98	2.03	26.59	2.17	2.23	30.19	2.41	2.48	34.90
	20	1.65	1.69	21.15	1.80	1.83	23.50	1.96	2.01	26.44
	∞	1.54	1.57	19.33	1.66	1.69	21.32	1.80	1.84	23.77
1	0	3.87	4.10	95.38	4.48	4.77	142.61	5.30	5.72	282.51
	5	1.97	2.01	26.10	2.14	2.19	29.15	2.34	2.40	33.00
	20	1.63	1.66	20.56	1.75	1.79	22.52	1.89	1.93	24.90
	∞	1.51	1.53	18.71	1.61	1.64	20.36	1.73	1.77	22.33
1.25	0	3.87	4.09	91.88	4.40	4.68	128.26	5.09	5.47	212.30
	5	1.96	2.00	25.72	2.11	2.16	28.36	2.28	2.34	31.60
	20	1.61	1.64	20.10	1.71	1.75	21.78	1.83	1.87	23.77
	∞	1.48	1.51	18.23	1.57	1.60	19.64	1.68	1.71	21.29
1.5	0	3.87	4.08	89.26	4.34	4.61	118.70	4.94	5.28	177.09
	5	1.95	1.99	25.41	2.08	2.13	27.74	2.24	2.29	30.54
	20	1.59	1.62	19.74	1.69	1.72	21.21	1.79	1.83	22.91
	∞	1.46	1.49	17.86	1.54	1.57	19.08	1.64	1.67	20.49

Table 6. Velocity response.

n	k	**Peak Velocity**								
		$P = 0$			$P = 1.32$			$P = 2.64$		
		$\rho = 0.001$ ($\times 10^{-4}$)	$\rho = 0.01$ ($\times 10^{-3}$)	$\rho = 0.1$ ($\times 10^{-3}$)	$\rho = 0.001$ ($\times 10^{-4}$)	$\rho = 0.01$ ($\times 10^{-3}$)	$\rho = 0.1$ ($\times 10^{-3}$)	$\rho = 0.001$ ($\times 10^{-4}$)	$\rho = 0.01$ ($\times 10^{-3}$)	$\rho = 0.1$ ($\times 10^{-3}$)
0.5	0	1.68	1.78	46.69	2.05	2.21	93.10	2.62	2.88	15,610.00
	5	1.42	1.45	19.35	1.58	1.62	22.47	1.78	1.83	26.79
	20	1.31	1.33	16.99	1.44	1.47	19.24	1.59	1.64	22.19
	∞	1.26	1.29	16.15	1.38	1.41	18.14	1.52	1.56	20.70

Table 6. *Cont.*

n	k	Peak Velocity								
		$P = 0$			$P = 1.32$			$P = 2.64$		
		$\rho = 0.001$ ($\times 10^{-4}$)	$\rho = 0.01$ ($\times 10^{-3}$)	$\rho = 0.1$ ($\times 10^{-3}$)	$\rho = 0.001$ ($\times 10^{-4}$)	$\rho = 0.01$ ($\times 10^{-3}$)	$\rho = 0.1$ ($\times 10^{-3}$)	$\rho = 0.001$ ($\times 10^{-4}$)	$\rho = 0.01$ ($\times 10^{-3}$)	$\rho = 0.1$ ($\times 10^{-3}$)
0.75	0	1.76	1.86	45.45	2.08	2.22	75.50	2.54	2.76	222.77
	5	1.43	1.47	19.23	1.57	1.61	21.83	1.74	1.79	25.25
	20	1.31	1.34	16.78	1.42	1.46	18.64	1.56	1.59	20.97
	∞	1.26	1.29	15.91	1.37	1.39	17.55	1.49	1.52	19.57
1	0	1.81	1.91	44.58	2.09	2.23	66.66	2.48	2.68	132.05
	5	1.44	1.48	19.13	1.57	1.60	21.37	1.71	1.76	24.19
	20	1.32	1.34	16.62	1.41	1.44	18.20	1.53	1.56	20.12
	∞	1.27	1.29	15.73	1.36	1.38	17.12	1.46	1.49	18.78
1.25	0	1.85	1.96	43.93	2.10	2.24	61.33	2.43	2.62	101.51
	5	1.45	1.48	19.05	1.56	1.60	21.01	1.69	1.73	23.41
	20	1.32	1.34	16.49	1.41	1.43	17.87	1.50	1.54	19.50
	∞	1.27	1.29	15.59	1.35	1.37	16.79	1.43	1.46	18.20
1.5	0	1.88	1.99	43.43	2.11	2.24	57.75	2.40	2.57	86.17
	5	1.46	1.49	18.99	1.56	1.59	20.73	1.67	1.71	22.82
	20	1.32	1.34	16.38	1.40	1.43	17.60	1.49	1.52	19.02
	∞	1.27	1.29	15.47	1.34	1.36	16.53	1.42	1.44	17.75

Table 7. Acceleration response.

n	k	Peak Acceleration								
		$P = 0$			$P = 1.32$			$P = 2.64$		
		$\rho = 0.001$ ($\times 10^{-3}$)	$\rho = 0.01$ ($\times 10^{0}$)	$\rho = 0.1$ ($\times 10^{0}$)	$\rho = 0.001$ ($\times 10^{-3}$)	$\rho = 0.01$ ($\times 10^{0}$)	$\rho = 0.1$ ($\times 10^{0}$)	$\rho = 0.001$ ($\times 10^{-3}$)	$\rho = 0.01$ ($\times 10^{0}$)	$\rho = 0.1$ ($\times 10^{0}$)
0.5	0	182.09	1.93	50.58	221.92	2.39	100.85	284.05	3.12	16,900.00
	5	251.58	2.58	34.35	280.04	2.88	39.89	315.76	3.26	47.55
	20	252.57	2.58	32.83	277.60	2.84	37.20	308.15	3.16	42.89
	∞	252.44	2.58	32.30	276.21	2.82	36.29	304.92	3.12	41.41
0.75	0	198.89	2.11	51.47	235.03	2.52	85.49	287.24	3.12	252.23
	5	258.64	2.65	34.74	283.85	2.91	39.45	314.49	3.24	45.63
	20	260.05	2.65	33.24	282.10	2.88	36.93	308.23	3.16	41.55
	∞	260.16	2.65	32.73	281.04	2.87	36.10	305.57	3.12	40.25
1	0	211.48	2.24	52.06	244.35	2.61	77.83	289.33	3.12	154.19
	5	264.12	2.70	35.04	286.73	2.94	39.13	313.57	3.22	44.30
	20	265.77	2.71	33.55	285.45	2.91	36.75	308.28	3.15	40.62
	∞	266.03	2.71	33.04	284.63	2.90	35.96	306.04	3.12	39.45
1.25	0	221.27	2.34	52.48	251.32	2.67	73.25	290.82	3.12	121.25
	5	268.50	2.74	35.27	288.99	2.96	38.89	312.86	3.21	43.34
	20	270.28	2.75	33.78	288.05	2.94	36.61	308.32	3.15	39.94
	∞	270.63	2.75	33.29	287.40	2.93	35.86	306.39	3.12	38.87
1.5	0	229.10	2.42	52.79	256.72	2.72	70.20	291.92	3.12	104.73
	5	272.07	2.78	35.45	290.80	2.98	38.70	312.30	3.20	42.60
	20	273.94	2.79	33.97	290.13	2.96	36.50	308.35	3.15	39.43
	∞	274.35	2.79	33.48	289.61	2.95	35.78	306.67	3.12	38.43

5.3. Structural Response Interpretation

It is possible to realize that as the rotational stiffness k increases, the structural response diminishes in a non-linear way for the different levels of the top axial load and self-weight.

Considering the spring coefficient, we can see that for values $k = 0$ to 5, the displacement drops by 50%, meaning that this range can produce significant influence on the structural response. For higher levels of k, a relative benefit is obtained in terms of the structural response. When the column is close to collapse due to buckling ($P = 2.64$, $n = 0.5$, $\rho = 0.1$), the displacement, velocity, and acceleration tend to be extremely large, indicating that the column is about to lose stability. The exact limit for the top load is 2.6479215086519375 ($n = 0.5$, $\rho = 0.1$). At this level of axial force, the frequency is zero (0.00).

It is possible to observe that for columns with low to moderate density, the accelerations increase until the first rotational stiffness is applied, decreasing further as the stiffness coefficient increases. For columns with high density, the accelerations decrease continuously from the hinged boundary condition, approaching convergency for coefficients close to 20. The structural response in terms of displacement and velocity follows the same pattern of behavior, independently of the applied loads and material density, decreasing constantly as the rotational spring coefficient increases.

Once the lateral forces are obtained ($F = Ku$), the bending moment can be calculated. The stress is obtained through the superposition principle, accounting for the action of the axial force—computing both lumped and distributed forces. For buildings, the maximum interstory drift permitted by Eurocode 8 [9] depends on the structural system adopted and building material. For normal buildings, the drift ratio limit is between 1% and 1.5% of the story height. The drift ratio defines the necessity of considering second-order effects like P-Δ calculation.

6. Conclusions

This work investigated the dynamic behavior of columns with variable cross-sections when they are subjected to earthquake loading. In the analysis, the change in the boundary stiffness was evaluated with a fast and simple one-degree-of-freedom model based on the generalized stiffness and mass of the structure. Several conclusions can be drawn:

- The natural frequency is significantly influenced by axial loading. The axial load is associated with the geometric stiffness parcel of the total generalized stiffness of the column. This means that the transversal stiffness of the columns, which is related to the lateral motion, does not depend on elasticity, but on its reluctance to change geometry, and is said to be exclusively geometric. The axial force of compression decreases stiffness and the vibration frequencies.
- Associated with the effect of axial force, it could be observed that when the density of the material increases by ten times, the frequency of the column decreases by around three times in relation to the previous value. For the same density, when the column changes shape, the frequency grows by different percentages. For $P = 0$, 1.91, 2.07, and 4.05 percent differences are found. For $P = 1.32$, these values are 3.71, 3.93, and 6.60. For $P = 2.64$, they are 5.79, 6.06, and 9.65.
- On the other hand, the combination of the top load equal to 2.64, considering two decimals, and the density of the material equal to 0.1 establishes the limit of axial loading to make the hinged–hinged column exist ($n = 0.5$). The exact value for the limit of the top load is 2.6479215086519375. At this level of force, the column frequency is zero (0.00). In this condition, the relationship between the top load and the total self-weight of the column is 0.3 ($n = 0.5$, $\rho = 0.1$). This is an important aspect that can be used in analysis by designers and researchers.
- The natural frequency depends on the shape of the column. The shape of the column is represented in formulations by the variable moment of inertia, $I(y)$. The shape variation of the column influences both the mass distribution and the axial force, $N(y)$, with repercussions for the geometric stiffness parcel and generalized mass of

the column. At the same time, the moment of inertia is also considered inside the generalized flexural stiffness parcel—K_0 of the total generalized stiffness, K. Therefore, several parameters are affected by the changing shape of the column, altering the structural response under seismic action.

- The natural frequency depends on the boundary conditions of the column. The boundary condition influences the total generalized stiffness of the structural system because it depends on the shape function assumed to represent the vibrational mode as well as the energy added by the rotational spring fixed to the base extremity. In this sense, the rotational spring alters the generalized stiffness through the shape function, and it provides an additional parcel of stiffness.
- Under seismic action, lower values of rotational base spring coefficients—around 5—reduce the displacement by around 50%, meaning that this range can exert significant influence on the structural response. For higher values, the reduction is not as significant.
- Under seismic action, when the column is close to buckling ($P = 2.64$, $n = 0.5$, $\rho = 0.1$), the peak displacement, velocity, and acceleration increase, signaling that the column is near to losing the stability.

Further studies are recommended to investigate the seismic response of columns with variable cross-sections of different shapes. Additionally, it would be desirable to analyze buildings using an equivalent system composed of generalized stiffness and mass parameters. Another avenue for exploration involves the application of rotational springs at both ends of the columns, in combination with rotational springs applied also to both shape functions. Experimental validation is also encouraged as a potential direction for future investigations. However, it is important to note that conducting experimental investigations requires careful planning, which always includes the development of sketches and executive drawings, buying or building specialized devices, precise specification of systems and sensors, acquisition of financial resources, obtaining support, booking laboratories, and engaging qualified personnel, among other actions.

Author Contributions: Conceptualization, A.d.M.W. and M.E.; Methodology, A.d.M.W. and M.E.; Software, A.d.M.W., C.B.E. and L.A.M.F.; Validation, A.d.M.W., M.E. and C.B.E.; Formal analysis, A.d.M.W., M.E., C.B.E. and L.A.M.F.; Investigation, A.d.M.W., M.E., C.B.E. and L.A.M.F.; Writing—original draft, A.d.M.W., C.B.E. and L.A.M.F.; Writing—review & editing, M.E.; Supervision, M.E.; Funding acquisition, A.d.M.W. All authors have read and agreed to the published version of the manuscript.

Funding: The first author thanks the National Council for Scientific and Technological Development (CNPq) of Brazil for his research scholarship given by the grant number 302494/2022-7.

Data Availability Statement: The original contributions presented in this study are included in the article. Further inquiries can be directed to the corresponding author.

Conflicts of Interest: The authors declare no conflict of interest.

Symbols and Abbreviations

A	cross-sectional area, m^2
a, b	shape function indication
b	column width
cos	cosine function
d	differential
( )	function
d( )/d	first derivative of a function

$d^2(\,)/d^2$	second derivative of a function
E	modulus of elasticity of a material, N/m^2
G	total self-weight, N
g	acceleration of gravity, m/s^2
I	moment of inertia of area, m^4
i	location along the column
K	total generalized stiffness, N/m
K_g	generalized geometric stiffness, N/m
K_0	generalized flexural stiffness, N/m
K_{ri}	generalized stiffness of a rotational spring, N/m
kg	kilogram
M	generalized mass, kg
m	meter
m^*	self-mass, kg
m_p	concentrated mass of a force P, kg
N	normal force, Newton (kg·m/s^2)
n	shape ratio
P	concentrated force, N
rad	radian
s	second
sin	sine function
y	geometric independent variable, m
γ	specific weight of the material, N/m^3
γ_p	coordinate of a force P, m
π	3.14159...
κ	rotational spring coefficient, N/m
φ	shape function
ω	natural frequency, rad/s
%	percent, 1/100
0, 1	boundary condition location

References

1. Santos, J.B.; Silva, T.J.; Salva, G.M. Influence of the stiffness of beam-column connections on the structural analysis of reinforced concrete buildings. *Rev. IBRACON Estrut. Mater.* **2018**, *11*, 834–855. [CrossRef]
2. Liang, L. Seismic behavior of irregular shaped beam-column connections. *Eng. Struct.* **2023**, *297*, 116942. [CrossRef]
3. Yu, M.; Yang, C.; Li, Y. Big Data in Natural Disaster Management: A Review. *Geosciences* **2018**, *8*, 165. [CrossRef]
4. Xie, B.; Wu, L.; Sun, L.; Xu, Y.; Yoshikawa, A.; Mao, W. Mechanism of Multiple Anomalies Prior to Japan Earthquakes from 2021 to 2023: Lithosphere-Coversphere-Atmosphere-Ionosphere Coupling Driven by Pressure-Stimulated Rock Current. *ESS Open Arch.* **2025**. [CrossRef]
5. Annapurna, D.; Yaqubi, E.; Anuradha, P.; Radhika, K. Seismic response of RC framed irregular structures. *Mater. Today Proc.* **2023**, *93*, 530–537. [CrossRef]
6. Chen, Z.; Liu, Y.; Zhong, X.; Liu, J. Rotational stiffness of inter-module connection in mid-rise modular steel buildings. *Eng. Struct.* **2019**, *196*, 109273. [CrossRef]
7. Liu, X.; Meng, Q.; Xu, L.; Liu, Y.; Tian, X. Modular Steel Buildings Based on Self-Locking-Unlockable Connections Seismic Performance Analysis. *Buildings* **2025**, *15*, 678. [CrossRef]
8. Zhang, J.; Yuan, W.; Zhang, T. Experimental study of earthquake resilient precast concrete beam-column-slab joints with bearing-double-stage energy dissipation connector. *Soil Dyn. Earthq. Eng.* **2025**, *190*, 109151. [CrossRef]
9. *EN 1998:2004*; Eurocode 8—Design of Structures for Earthquake Resistance: General Rules, Seismic Actions and Rules for Buildings. European Committee for Standardization (CEN): Brussels, Belgium, 2004.
10. Morano, M.; Liu, J.; Williamson, E.; Hutchinson, T.; Pantelides, C.; Saxey, B.; Richards, P. Shake table testing of a full-scale three-story seismically resilient steel-framed building with reconfigurable lateral force-resisting systems. *Earthq. Spectra* **2025**, *41*, 87552930241301424. [CrossRef]
11. Gorini, D.N.; Marrazzo, P.R.; Nastri, E.; Montuori, R. Effectiveness of an innovative seismic resilient superelevation in an archetype, existing soil-structure system. *Bull. Earthq. Eng.* **2025**, *23*, 1677–1705. [CrossRef]

12. Chanda, D.; Saha, R.; Haldar, S.; Choudhury, D. State-of-the-art review on responses of combined piled raft foundation subjected to seismic loads using static and dynamic approaches. *Soil Dyn. Earthq. Eng.* **2023**, *169*, 107869. [CrossRef]
13. Alva, G.M.S.; Debs, A.L.H.d.C.E.; El Debs, M.K. An experimental study on cyclic behaviour of reinforced concrete connections. *Can. J. Civ. Eng.* **2007**, *34*, 565–575. [CrossRef]
14. Kataoka, M.N.; Ferreira, M.A.; El Debs, A.L.H. Study on the behavior of beam-column connection in precast concrete structure. *Comput. Concr.* **2015**, *16*, 163–178. [CrossRef]
15. Choi, H.-K.; Choi, Y.-C.; Choi, C.-S. Development and testing of precast concrete beam-to-column connections. *Eng. Struct.* **2013**, *56*, 1820–1835. [CrossRef]
16. Xiong, X.; Wei, Z.; Zhang, D.; Liu, J.; Xie, Y.; He, L. An Experimental Study on the Seismic Performance of New Precast Prestressed Concrete Exterior Joints Based on UHPC Connection. *Buildings* **2025**, *15*, 729. [CrossRef]
17. Zhang, Z.; Guo, F.; Gao, J.; Deng, E.; Kong, J.; Zhang, L. Seismic performance of an innovative prefabricated bridge pier using rapid hardening ultra-high performance concrete. *Structures* **2025**, *74*, 108558. [CrossRef]
18. Ardalani, A.; Aydin, A.C. Nonlinear Seismic Performance Assessment of Energy-Based Steel Structures with Semi-Rigid Connections. *Iran. J. Sci. Technol. Trans. Civ. Eng.* **2025**, 1–32. [CrossRef]
19. Maali, M.S.; Tavlaşoğlu, M.E.; Maali, M. Experimental study on the cold-formed steel beam-to-column screw connections for seismic application. *Structures* **2025**, *72*, 108173. [CrossRef]
20. Xu, J.; Gan, Z. Post-earthquake fire resistance of beam-column connection connected with high-strength steel flush end-plate. *Structures* **2025**, *71*, 108190. [CrossRef]
21. Marmarchinia, S.; Azad, A.R.G.; Mirghaderi, S.R.; Karney, B.; Ali, M. A novel modular system for pipe racks using friction-slip connections. *J. Constr. Steel Res.* **2025**, *226*, 109286. [CrossRef]
22. Meng, B.; Li, H.; Liew, J.-Y.R.; Li, S.; Kong, D.-Y. Enhancing the Collapse Resistance of a Composite Subassembly with Fully Welded Joints Using Sliding Inner Cores. *J. Struct. Eng.* **2024**, *150*, 04024085. [CrossRef]
23. Strutt, J.W. *The Theory of Sound*; Re-issued 1945; Dover Publications: New York, NY, USA, 1877; Volume 1, p. 544.
24. Wahrhaftig, A.d.M.; Magalhães, K.M.; Silva, M.A.; Brasil, R.M.d.F.; Banerjee, J.R. Buckling and free vibration analysis of non-prismatic columns using optimized shape functions and Rayleigh method. *Eur. J. Mech. A/Solids* **2022**, *94*, 104543. [CrossRef]
25. Banerjee, J.; Jackson, D. Free vibration of a rotating tapered Rayleigh beam: A dynamic stiffness method of solution. *Comput. Struct.* **2013**, *124*, 11–20. [CrossRef]
26. Ghani, S.N.; Neamah, R.A.; Abdalzahra, A.T.; Al-Ansari, L.S.; Abdulsamad, H.J. Analytical and numerical investigation of free vibration for stepped non-homogeneous cantilever beam. *Open Eng.* **2022**, *12*, 184–196. [CrossRef]
27. Peng, S.; Xiong, Z.; Xu, C.-X.; Fei, J.; Chen, X. Research on shear strength of CFSST column and H-section with beam composite joint of unequal depth. *J. Constr. Steel Res.* **2021**, *180*, 106575. [CrossRef]
28. Poudel, P.; Adhikari, B. Comparative Study on Seismic Behavior of Regular and Irregular Building in Sloping Ground. *Himal. J. Appl. Sci. Eng.* **2025**, *5*, 105–123. [CrossRef]
29. Xu, Z.-H.; Bai, G.-L.; Zhao, J.-Q.; Liu, B. Study on seismic performance of SRC leaning beam-column exterior joints in the main workshop of CAP1400 nuclear power plant. *Structures* **2021**, *34*, 2721–2734. [CrossRef]
30. Wang, B.; Dai, H.; Wu, T.; Bai, G.; Bai, Y. Study on seismic performance and influencing parameters of SRC exterior joints with the variable column in main building for thermal power plants. *Earthq. Eng. Eng. Dyn.* **2014**, *34*, 86–96.
31. Zhou, Y.; Wang, X. A methodology for formulating dynamical equations in analytical mechanics based on the principle of energy conservation. *J. Phys. Commun.* **2022**, *6*, 035006. [CrossRef]
32. Espí, M.V.; Bravo, J.C.; Rojas, C.O. On Galileo's Tallest Column. *Math. Probl. Eng.* **2015**, *2015*, 649341. [CrossRef]
33. Eisenberger, M.; Wahrhaftig, A.d.M. Buckling Loads of Variable Stiffness Columns Loaded by Top Load and Linearly and Parabolically Distributed Loading. *Int. J. Struct. Stab. Dyn.* **2024**, *5*, 2650001. [CrossRef]
34. Ilanko, S.; Monterrubio, L.E.; Mochida, Y. *The Rayleigh—Ritz Method for Structural Analysis*; John Wiley & Sons, Inc.: Hoboken, NJ, USA, 2014.
35. Piyapiphat, S.; Nuntasri, A.; Phungpaingam, B.; Musiket, K.; Jiammeepreecha, W.; Chucheepsakul, S. Influence of self-weight on buckling and post-buckling behavior of AFGM spring-hinged cantilever column under tip load. *Mech. Based Des. Struct. Mach.* **2025**, 1–25. [CrossRef]
36. Wang, Y.; Lv, J.; Yang, M.; Zhang, Y.; Qin, T.; Wang, L. Stability analysis of an articulated flexible pipe conveying fluid with a rotational spring. *J. Fluids Struct.* **2025**, *133*, 104277. [CrossRef]
37. Wahrhaftig, A.d.M.; Eisenberger, M. Buckling load of heavy columns with variable cross section and flexible end restraints. *Zamm* **2024**, *104*, e202400626. [CrossRef]

Disclaimer/Publisher's Note: The statements, opinions and data contained in all publications are solely those of the individual author(s) and contributor(s) and not of MDPI and/or the editor(s). MDPI and/or the editor(s) disclaim responsibility for any injury to people or property resulting from any ideas, methods, instructions or products referred to in the content.